Wave-induced Force Dynamics Analysis of Tension Leg Platform

M I Adam [1] *

E J Chong [1]

[1] *Formally, at Department of Mechanical Engineering, NEU, Malaysia*

ABSTRACT

This work analyses the dynamic response of Tension Leg Platform, TLP under sea wave induced forces with the aid of fluid dynamics modified Morison equation, single degree of freedom mass spring damper theory, and the Runge-Kutta ode45. Specifically, we employ the modified Morison equation to calculate the sea wave forces acting on a cylinder hull of the TLP. Two types of sea wave characteristics are analysed including sea waves in the South China Sea to compute the waves loading on the hull. Evaluated results are incorporated into the equation of motion of the platform, modeled as a single degree of freedom mass-spring-damper system to obtain the platform displacement at x-axis direction. The results showed that the dynamic response of the platform under the influence of sea wave A exhibits a displacement of 0.02 m in the direction of wave propagation parallel to the x-axis of the platform. Meanwhile, sea wave B manifests a magnitude at least twenty times larger compared to sea wave A, resulting in 0.5 m displacement in the same axis direction. We further examine the consequence of velocity profile of sea waves on displacement and time taken for a complete vibrational cycle. A parameter-fed CFD simulation with Star-CCM+ shows clear dynamic response of the TLP when acted upon by sea wave A. Obtained results indicate the importance of materials selection for construction of the hull tendons based on the motion of the hull and gives a fair estimate for cyclic loading on the tendons throughout the life cycle of the platform.

Keyword: TLP platform; hull tendons; drag and inertia forces.

INTRODUCTION

Tension Leg Platform, TLP is a floating platform structure widely used in oil exploration all over the world. It is designed to operate at deep water region of underwater depth ranging from 500 m to 1500 m. TLP consists of four parts which are the tendons, skiddable platform rig, hull, and production risers. The structure is moored by steel pipes connected to seabed and is aligned vertically with the semi-submersible hull. These steel pipes or tendons are always in mechanical tension due to excess buoyancy in the structure causing the platform to float in upward direction. The pre-tensioned tendons installation prevents vertical motion of the TLP floating structure. Production facilities were situated in the skiddable platform rig above the surface level of the sea. The production facilities contain different complex systems, fuel gas, gas compression, water injection pump, and crane. The platform rig also houses living quarters and pedestal crane on the main deck. Fuel gas skid, and air compressor packages on the mezzanine deck, open caisson pump and wellhead situated on the production deck. The hull is semi-submersible and comes in varies designs. The production risers serve to transport materials from seafloor to production

facilities on the sea surface and vice versa. In TLP, the design of top-tensioned risers allows for vertical termination below the facility. Similar to pipelines or flowlines, risers transport materials such as the explored hydrocarbon, injection fluids, and gas lift. Risers are rigid or flexible in structure, and especially insulated to withstand seabed temperature.

To construct this mammoth structure, design engineers have to perform critical engineering analysis for tendons using theories such as the Pythagorean Theorem, Stress-Strain, and the Young's Modulus relationships. It is possible to locate the strain of the tendons using Pythagorean Theorem with platform horizontal displacement and water depth as the legs of the triangle, and the strain as the hypotenuse. By calculating the stress distribution on the vertical section of the tendons, the stress-strain relationships can be used to obtain the Young's Modulus required by the system to match with the materials' one. Conventionally, the material of the tendons used in the TLP construction is watertight hollow composite semi-flexible steel pipes, known for reducing the overall submerged weight of the tendons. However, as the water depth increases, the thickness of the steel pipe requires further solidifying to withstand a greater hydrostatic pressure. Increase in thickness leads to increase in tendon weight, which in turn reduces the axial stiffness of the tendons that holds the platform in position. Therefore, the question to predict the horizontal movement of the platform opens up the possibility to determine whether the existing tendons are able to support a platform built in for example, the South China Sea environment.

Wave-induced force dynamics analysis of the TLP has caught the attention of many researchers due to the importance of TLP in deep-water oil and gas exploration [1-15]. Hence, dynamics analysis is required to determine and therefore, minimize sea wave impact on the underside of the deck. This is to regulate the sea wave low frequency horizontal force motion and, to avoid slack of tendons. It is also critical to determine the dynamics on the TLP in order to prevent snapping of tendons and risers in such an active environment. Generally, the TLP behaves like an inverted pendulum with sufficient buoyancy force acting on the hull to maintain the tendons' tension. However, after 900 m sea depth, the size of the TLP increases remarkably to accommodate the sway natural period of deep water to prevent slacking of tendons. With its size increases, the magnitude of first and second order sea wave forces acting on the hull structure increases significantly. As a result, the cost of constructing the TLP increases as its size increases thus, it brings incredible debt to the rig owner. One solution to this problem is to determine the dynamic response of the TLP due to wave-induced vibration forces in order to obtain an estimate frequency to guarantee safety of the structure and scale down the costs. To calculate the dynamic response of TLP, we use the classic theory of single degree of freedom system to determine the vibrational behaviour of the structure. This work also investigates the sea wave load on TLP using modified Morison equation and simulate the dynamic response of a TLP acted upon by hydrodynamic sea wave loading. We compute the drag force and the inertia force components on the TLP and determine the empirical hydrodynamic coefficients for both forces. Once the sea wave forces on TLP have been determined, the next

objective is to calculate the resulting response of the structure as a function of time. Note that his work only covers the horizontal displacement of the structure taken as positive in the direction of sea wave propagation. We assume that the vertical displacement of the structure is negligible due to the design nature of TLP that has tensioned tendons, which restrict the vertical movement of the structure. This work does not cover force-induced structure displacement due to wind forces as the wind forces categorize as static. We limit our investigation to sea waves impinging normal to the face of a cylinder hull structure of the TLP. This is to limit the overly complicated calculations involving platform rotation when the wave propagation is not parallel to the cylinder hull.

LITERATURE REVIEW

There have been patents generated for the TLP regarding its overall structure and mooring systems. H. A. Bourne et al. [1] described in detail the advantage of using TLP over concrete structure due to the deep-water height. He stressed the importance of vertical mooring system components to be reliable, inspectable, and replaceable throughout the platform life cycle. Thus, his patent revolved around the design of the tension legs, which consist of individual threaded steel tubular tension leg rods. The proclaimed design allows for easily removal of rods for inspection. Replacement or reinsertion of new tensioned-rods with simple and readily available equipment on board the platform may take place without the need for an extra hand from onshore. D. I. Karsan [3] added mass stabilizer system for the TLP in order to control the first order multiple direction movements of the platform. The stabilizer is designed to fit beneath the platform at an appropriate distance between the hull and seabed to minimize the pitch and roll torqueing with sufficient flexibility to avoid shock load by sea waves. The stabilizer, sized according to the size of the platform and sea depth to provide sufficient submerged weight to maintain the platform tendons in constant tension while controlling the platform motion. S. R. II. William [4] proposed a design that could improve the hydrodynamic performance of the TLP. The design includes a hull with four radially oriented columns connected with four rectangular pontoons. The pontoons allow the mooring system with tendons to connect directly at the lower corner of the column instead of the base of the pontoons. This patent highlights an important method to increase the stability of the platform installation via a temporary buoyancy module to keep the pontoons from moving due to sea waves before securing it to a mooring system and de-ballasted.

TLP is typically modelled as a rigid body having three translations (surge, sway, and heave), and three rotations (roll, pitch, and yaw), a six-degree-of-freedom motion. However, recent study by A. A. Taflanidis [5] assumed that sea wave propagation direction is parallel to the axis of symmetry of the TLP. Such an assumption limits the sway, roll, and yaw motions of the platform leading to only surge (x), heave (z), and pitch (θ) motions with three-degree-of-freedom. On the other hand, A. K. Jain [6] took another approach by considering all six-degree-of-freedoms' in a nonlinear dynamic analysis of TLP under general conditions

where wave force is parallel with the axis of symmetry of the TLP. He concluded that fluctuation in tension of tendons is large due to possible heave period close to the frequently occurring wave periods. H. H. Lee [7] considered a complete analytical solution of the dynamic behaviour of TLP structure with tendons when subjected to wave-induced surge motion and flow-induced drag motion. Their general equation of motion employs Newton's second law. The motion of tendons subject to wave-induced forces and surge motion thus far calculated using Morison's equation for a small body taking into consideration the scattering and radiation effects produced by sea wave. This work found that the traditional analysis of TLP without considering the effect on tendons overestimates the vibration amplitude of the TLP. Unlike conventional analysis, Adrezin & Benaroya [8] undertook an interesting approach by modelling the equation of motion and response of the TLP undergoing planar motion with only a single tendon pinned to the hull and the sea floor instead. They modelled the hull as rigid cylindrical body and the single tendon as nonlinear elastic beam. However, modelling of single tendon attached to the hull does not give accurate dynamic response as well as it eventually offset the pitch response of the structure compared to full tendons arrangement.

Harleman *et al*. [9] reported the dynamic analysis of offshore structure focusing on structure with four legs in a square configuration using "statical" wave force analysis. In their experimental platform constructed of plastic placed in a wave tank, the highest expected wave is not the critical design wave whereas the smaller waves with resonance periods have caused twice as high a displacement of the platform. They concluded that smaller waves having periods close to resonance response of the platform causes maximum displacement and structural stresses. S. M. G. Zadeh *et al*. [10] recently performed a nonlinear response analysis of fixed offshore platform under a combined force of waves, wind, and sea current. They used Morison equation to compute the wave force acting on the structure. Their finite element analysis approximates a solution for the equations governing the continuous areas to obtain the structure displacement. A. A. M. Ali *et al*. [11] used a similar approach for a generalized Morison equation to calculate the wave load.

However, they applied wave load on two different wave theories of the Airy's linear theory, and Second Order Stoke's theory in order to obtain the dynamic analysis of the structure.

By comparing both wave theories, they concluded that both linear and second order wave theories showed almost identical behavioural response on the platform. The Airy's linear theory however generally reduces the computational costs.

Realistically, sea wave profile varies for different locations and these profiles can be completely random at different times. One of the most feared wave profiles to act on offshore structures is the rogue wave profile. Rogue wave is an unpredictable wave, greater than twice the size of the surrounding waves and, often time comes unexpectedly from directions other than the prevailing wind and waves [12]. In 2005, Shell Mars TLP was hit by Hurricane Katrina, which has resulted in an estimate of 300 million dollars in damage

and one-year production downtime [13]. In recent study, M. Rudman & W. P. Cleary [14] have included the rogue wave impact on the TLP by looking into the effect of wave incidence angle and mooring line tension. They utilized the Smooth Particle Hydrodynamic, SPH method to simulate a nonlinear dynamic of large wave to observe the effect it has on the TLP. Their study concluded that major platform motion occurred during the initial wave impact while the impact of subsequent wave decreases with time. This impact resulted in significant pitch motion within the first four seconds of the wave hit followed by significant surge motion that led to tendons and risers undergoing large strains. Similarly, T. B. Johannessen *et al*. [15] examined the so-termed badly behaved problem of a TLP because of extreme wave effect. Their research focused on determining the TLP tendons loading using improved Volume of Fluid, iVOF software instead of dynamic response of the platform. Yet, their paper gave an insightful view of TLP tendon loading mechanism that sets the standards for tendons response to abnormal sea wave conditions. In addition, Wu *et al*. [2] successfully modelled the TLP motion in extreme wave event using Computational Fluid Dynamics, CFD simulation software. Their results showed positive similarity with model test measurement except for initial conditions where low frequency waves are involved. They also highlighted that CFD software had effectively captured the ringing response in tendons tension induced by higher order nonlinear wave dynamics.

MORISON EQUATION

Morison's equation [16] has been used to calculate the hydrodynamic drag and inertia forces since [17]. Its accuracy in determining the wave load on cylindrical structure has shaped most of the existing platform structures today. Morison equation contains two different empirical hydrodynamic coefficients each exists in individual equation. The drag coefficient, usually known by the symbol C_d whereas the inertia coefficient is C_m. Chandrasekaran [18] conducted a study on the influence of these coefficients on nonlinear response behaviour of TLP under regular waves. The study concluded that C_d and C_m have principal effect on determining the dynamic behaviour of the TLP. The range selection of hydrodynamic coefficients due to water depth greatly affects the results of dynamic analysis of the TLP. Standardized Morison equation of force per unit length F' can be defined as shown below.

$$F' = F_{drag} + F_{inertia} = \frac{1}{2} \rho\, C_d D \dot{u}|\dot{u}| + \frac{\pi}{4} r C_m D^2 \ddot{u} \qquad (1)$$

where ρ is fluid density or the density of sea water, D is cylinder diameter of the hull, $\dot{u}$ is incident flow velocity of the sea wave, C_d is hydrodynamic drag coefficient, C_m is hydrodynamic inertia coefficient, and $\ddot{u}$ is the incident flow acceleration. Successful computation of the horizontal wave force against phase angle with C_d value of 1.2 and, C_m value of 2.0 were performed [9]. R. Burrowsa *et al*. [19] obtained an estimate for C_d and C_m values for random seas applied to Morison equation using different analytical methods including least-squares analysis, cross-spectral analysis, and methods of moments. They successfully produced the non-

dimensional force against time graphs for random sea waves. The hydrodynamic forces acting on the hull of a TLP is considered as force acting on a slender structure in fluid flow by commuting the summation of all sectional forces acting on each strip of the structure. Among the forces considered are normal force, tangential force, and lift force. The lift force is normal to both normal and tangential forces. In general, Morison equation is only valid if the diameter of cylinder hull is relatively small compared to the wavelength such that $D/\lambda \leq 0.2$ [20] where D is the diameter of the cylinder hull, and λ is the wavelength where both quantities are measured in metres. Based on Environmental Conditions and Environmental Loads Recommended Practise Handbook [21], the drag coefficient C_d is non-dimensional,

$$C_d = \frac{f_{drag}}{0.5\rho D v^2} \qquad (2)$$

where f_{drag} (N/m) is the sectional drag force, ρ (kg/ m^3) is the fluid density, D (m) is the diameter of the hull and v (m/s) is the velocity of the traveling wave.

The inertia coefficient C_m is the non-dimensional added mass

$$C_m = 1 + \frac{m_a}{\rho A} \qquad (3)$$

where m_a (kg/m) is the added mass per unit length and A (m^2) is the cross-sectional area of the hull.

METHOD

The equation and assumptions made so far, and hereafter, are based on dynamic analysis of a TLP tethered by four tensioned tendons and acted upon by a series of oscillatory sea waves. The horizontal displacement denoted by the unknown X, measured from the centre of the base of the TLP situated on the surface of the sea. The equation of motion of a single degree-of-freedom, spring-mass system with linear damping under harmonic force is as below.

$$m\frac{d^2X}{dt^2} + C\frac{dX}{dt} + KX = F'(t) \qquad (4)$$

$$m\,\ddot{x}(t) + c\,\dot{x}(t) + k\,x(t) = F'(t)$$

where m (kg) is the effective mass of system of TLP and tendons, C (Ns/m) is the damping coefficient of the system, K (N/m) is the spring constant of the system, and F' (N) is the hydrodynamic force acting upon the TLP in terms of time calculated via Morison's equation. If the single degree of freedom system is forced with a sinusoidal force function, the value of $F'(t)$ can be represented by $f\cos(\omega t)$ where ω is the frequency of the force. In this case, the frequency of the force in the sinusoidal function is the frequency of the sea wave forcing on the cylinder hull. If the value of $F'(t)$ continuously persists with time, then, the system responds only at the frequency of the sea wave, ω after several force cycles.

$$x(t) = X\cos(\omega t - \theta) \qquad (5)$$

where X and θ are undetermined constants denote the amplitude and phase angle of the response. By substituting equation (5) into equation (4), we obtain

$$X\,[\,k - m\omega^2)\cos(\omega t - \theta)$$
$$- c\omega\sin(\omega t - \theta)] = f\cos(\omega t) \qquad (6)$$

Equating the coefficients of $\cos\omega t$ and $\sin\omega t$ on both sides of the equation, we obtain

$$X[(k - m\omega^2)\cos\theta + c\omega\sin\theta\,] = f \qquad (7)$$

$$X[(k - m\omega^2)\sin\theta + c\omega\cos\theta\,] = 0$$

Replacing ω with σ for frequencies, the solution to equation (7) yields,

$$X = \frac{f}{K\sqrt{\left[1-(\frac{\sigma}{\sigma_n})^2\right]^2 + \left[2\frac{C\sigma}{C_c\,\sigma_n}\right]^2}} \qquad (8)$$

where X (m) is the horizontal displacement of the platform measured from the centre of the base, σ_n is the undamped natural frequency of the system which can be calculated using $\sqrt{k/m}$, σ is the frequency of sea wave, C_c is the critical damping coefficient which can be calculated using $2\sqrt{mK}$, and f is the force amplitude obtained by Morison equation. With reference to [5], a similar model of the TLP is created for the purpose of this work. Figure 1 shows a proposed model of TLP with four tendons connected to the base. The X (t), and –X (t) show the horizontal displacement of the platform measured from the centre of the platform. The value of F (t) shows the force acting on the tendons and cylinder hull. The L value shows the total water depth of the platform and the tendons length. The value of S is defined to determine the influence fraction value, which will be discussed later.
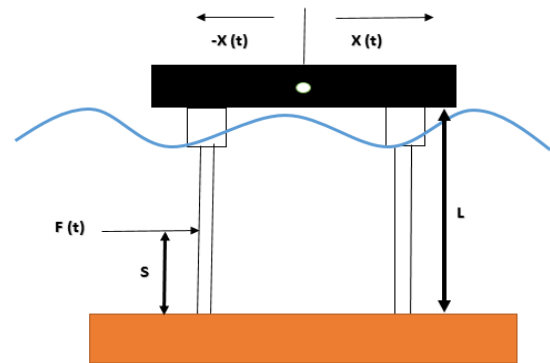

Figure 1: A schematic representation of TLP with four tendons connected to the base.

Based on Morison equation, both hydrodynamic drag force and the inertial force contribute to F (t). Thus, it cannot be presented in a single term of $F\sin(\sigma t)$ form. However, Fourier series approximation of F (t) represents a series of sine terms to any desired degree of accuracy. Since the

equation of motion is linear, the component displacement due to individual exciting force terms ($F sin(\sigma t)$), in the Fourier series can be summed up to determine the total platform displacement as a function of time.

$$X_{total}(t) = \sum X_{individual}(t) \qquad (9)$$

Modified cantilever beam theory used by D. R. F. Harleman [9] yields the static deflection of the tendons and platform. Based on Figure 1, the equation of maximum deflection of the deck $X_{max}(t)$ for a force F applied at an elevation S is

$$X_{max,act} = \frac{FS^2}{NEI}\left(\frac{L}{4} - \frac{S}{6}\right) \qquad (10)$$

In Equation (10), the value of S can be substituted for L should the evaluation made for the force F' applied on the platform base, resulting in

$$X_{max,equiv} = \frac{F\prime L^3}{12NEI} \qquad (11)$$

where E (GPa) is the elastic modulus of the TLP which is the elastic modulus of steel based on the eight giant steel tendons support buoy. I (kg.m^3) is the moment of inertia of TLP, N is the number of tendons in the system, which is 4 in this work, and L (m) is the length of the tendons.

In order to determine the relationships of forces F' and F, an influence fraction has been established by equating Equations (10) and (11) in the form of ratio $\frac{F\prime}{F} = f$. The f value represents the ratio of equivalent deflection over actual deflection of the platform. If the value of S is equal to L, the influence fraction f is equivalent to value of 1.0, which concludes that the value of F' is equal to F.

$$\frac{F\prime}{F} = f = 3\left(\frac{S}{L}\right)^2 - 2\left(\frac{S}{L}\right)^3 \qquad (12)$$

The spring constant of the system given by the Hooke's Law equation is $F = kX$. In this paper, the spring constant of the equivalent system is

$$K = \frac{F\prime}{X_{max,equiv}} = \frac{48EI}{L^3} \qquad (13)$$

The natural frequency of the equivalent system is the same as the natural frequency of the actual platform given the identical nature of both systems. D. R. F. Harleman [9] was able to calculate the natural frequency of similar system using the static deflection curve to determine the potential and kinetic energy values. Using the Rayleigh's Energy Method, he was able to compute the natural frequency by equalling the potential and kinetic energies. In this work, the natural frequency of the system is obtained by the following equation.

$$\sigma_n = \sqrt{\frac{K}{\frac{1}{g}(W + \frac{13}{35}NwL)}} \qquad (14)$$

where W (kg) is the weight of the platform, w (kg) is the weight of one tendon, $N = 4$ is the number of tendons, and L

(m) is the total length of the tendon. By comparing the conventional equation of natural frequency in terms of spring constant and mass, $\sigma_n = \sqrt{k/m}$ to equation (14), the effective mass of the system is found to be

$$m_{eff.} = \frac{1}{g}\left(W + \frac{13}{35}NwL\right) \qquad (15)$$

Accordingly, the critical damping coefficient, C_c can be determined with the following equation

$$C_c = 2\sqrt{m_{eff.}k} \qquad (16)$$

where $m_{eff.}$ is the effective mass of the system obtained, and k is the spring constant of the system. The damping coefficient can be calculated using logarithmic decrement method by determining the first and second successive positive displacement amplitudes of the platform in a complete cycle [22].

$$\varphi = \frac{C}{C_c} = \frac{1}{2\pi}\left(\ln\frac{X_1}{X_2}\right) \qquad (17)$$

where X_1 (m) is the first positive displacement of the platform under wave loading, and X_2 (m) is the second positive displacement of the platform under wave loading. The frequency of the force loading on the platform is the frequency of the harmonically exciting wave as defined by $\sigma = \frac{2\pi}{\tau}$.

where τ (s) is the period of the sea wave. The phase angle of the system can be calculated using the formula

$$\phi = \tan^{-1}\left[\frac{2\frac{C}{C_c}.\frac{\sigma}{\sigma_n}}{1-\left(\frac{\sigma}{\sigma_n}\right)^2}\right] \qquad (18)$$

where C is the damping coefficient obtained from equation (17), C_c is the critical damping coefficient obtained from equation (16), σ is the frequency of sea wave obtained from equation (8), and σ_n is the undamped natural frequency of the platform obtained from equation (14). The final form of the equation of motion taking into account Morison's equation and hydrodynamic force coefficients determines the overall platform displacement under the force induced by linear sea waves.

$$X(t) = \frac{\frac{\pi}{4}rC_mD^2a(\sin(\omega t))+\frac{1}{2}rC_dDv^2(\cos(\omega t))}{k\sqrt{\left[1-\left(\frac{\sigma}{\sigma_n}\right)^2\right]^2 + \left(2\frac{C\sigma}{C_c\sigma_n}\right)^2}} \qquad (19)$$

Based on equation (19), we conclude that the inertia coefficient C_m value, and drag coefficient C_d value determine the dominance of the drag and inertia forces. With C_m value higher than C_d, the term of the numerator of Equation (19) generates the majority of the force acting on the platform. On the other hand, if C_d value is higher, the drag force is deemed the greater contributor to the platform displacement. It is crucial to determine the platform characteristics mentioned beforehand according to different sea conditions. Different sea conditions contribute to several

variations in the equation such as wave velocity amplitude, sea wave frequency, and wave flow acceleration. However, average values of the said parameters can be obtained from the meteorological and marine departments of each jurisdiction. In the case of sea wave velocity amplitude, its variation can ranges from 20 m/s with period of 31 s to 30 m/s with period of 20 s on a normal wave basis depending on the wind speed and weather conditions. However, in the case of a high velocity waves caused by hurricane and bad weather conditions, the wave velocity amplitude can reach an unusually high velocity of 200 m/s and has a much smaller wave period of 12 s.

In order for the Runge-Kutta ode45 to accommodate Equation (19), we transform this equation into a simple ODE that has a single solution component, which specifies an anonymous function in the call to the solver. Hence, Equation (19) simplifies into

$$\frac{dy}{dt} = \frac{F_1 \sin \omega t + F_2 \cos \omega t}{G} = f(t, y) \qquad (19.1)$$

$$F_1 = \frac{\pi}{4} r C_m D^2 a \qquad (19.2)$$

$$F_2 = \frac{1}{2} r C_d D v^2 \qquad (19.3)$$

$$G = k \sqrt{\left[1 - \left(\frac{\sigma}{\sigma_n} \right)^2 \right]^2 + \left(2 \left(\frac{C\sigma}{C_c \sigma_n} \right)^2 \right)} \qquad (19.4)$$

The terms F_1 and F_2 represent the magnitude of inertia and drag forces computed using Morison equation, and G as the constant value derived from different platform characteristics. The single solution component value of $\frac{dy}{dt}$

obtained by solving the equation using ode45 represents the horizontal movement X of the TLP platform measured from the center of the base. With initial conditions y = y_0 = 0 at time t_0 = 0, the vector of functions $f(t, y)$ or Equation (19.1), the mathematical model specifies the platform characteristics with the predetermined parameters. With all the correct values input into ode45 functions, we regulate all variables for the equation of motion governing the platform displacement over a determined time span.

RESULTS AND DISCUSSION

We modify and develop a CFD mesh model based on the original CAD model [23]. A simulation of dynamic response of the TLP acted upon by sea wave *A* was developed using CFD simulation software, Star-CCM+ as shown in Figure 2. Based on Figure 2 (a), the simulation starts with zero displacement at t = 0 s. In Figure 2 (b), the wave begins affecting the platform at approximately t = 4.25 s. The platform surges toward the x-direction upon impact by the wave. While in Figure 2 (c), the platform exerts its maximum displacement at t = 8.02 s. The platform shows signs of heaving at this moment as the tendons cable pulls the platform back toward its original position. In Figure 2 (d), the platform returns to its original position at t = 14.06 s. When t = 20.15 s as shown in Figure 2 (e), the platform exhibits a negative displacement at x-direction due to the tendons restoring force on the platform. At t = 24.86 s, the platform returns to its original position at zero displacement at the same position shown in Figure 2 (a), and 2 (f), respectively.
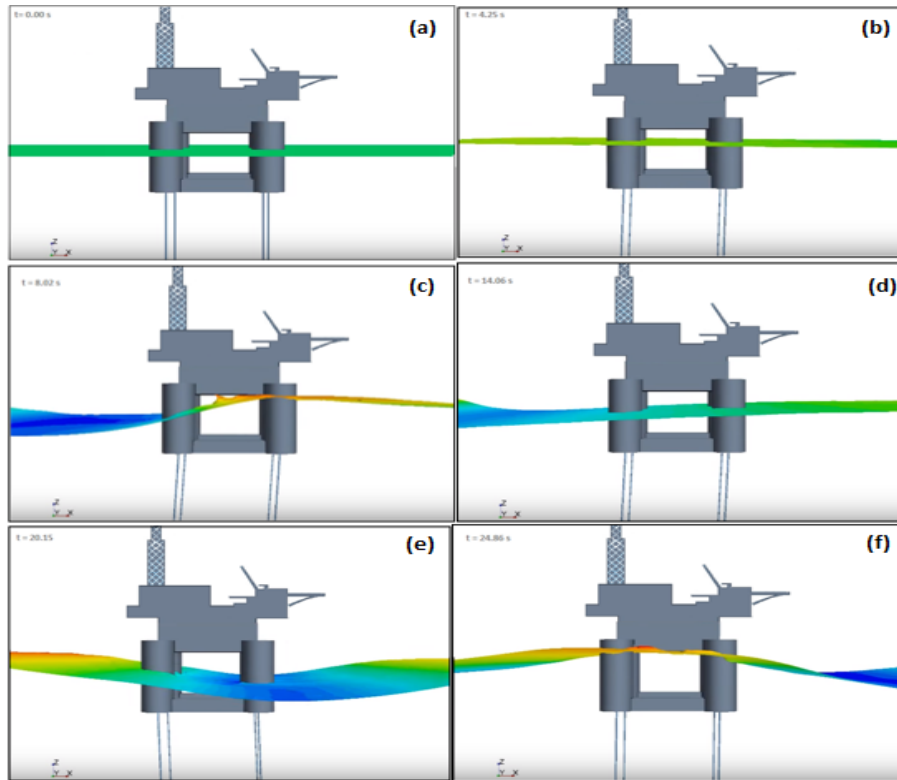

Figure 2: Dynamic response of the TLP platform acted upon by sea wave *A*.

The platform parameters used for the analysis in this work are based on the TLP constructed by SSPC and Technip-MMHE [24]. Weather conditions and sea wave parameters are based solely on several studies [25, 26]. Table 1 demonstrates some of the sea waves characteristics.

Table 1: Characteristics of two different waves. Platform and sea wave parameters collected from references shown in the text.

Unit	Wave *A*	Wave *B*
τ (s)	25	12
$\sigma = 2\pi/\tau$ (1/s)	0.251	0.253
$\ddot{u}$ (m/s^2)	~	~
σ (rad/s)	0.25	0.5
$\dot{u}$ (m/s)	25	200
λ(m)	625	2500

To validate our calculations using Morisons' equation we followed the steps stated in Ref. [20].
For sea wave *A*, the wave velocity amplitude at 25 m/s and sea wave frequency of 0.25 rad/s (~ 0.04Hz) produces a wavelength $\lambda = 625\ m$, and $\frac{D}{\lambda} = 0.08$, a value smaller than 0.2. For sea wave *B*, the wave velocity amplitude at 200 m/s and sea wave frequency of 0.5 rad/s (~ 0.08Hz) obtains a wavelength $\lambda = 2500\ m$, and $\frac{D}{\lambda} = 0.02$, once again, a value smaller than 0.2.
Thus, the above findings validate the use of Morison equation to compute the hydrodynamic force for both sea waves *A* and *B*, respectively. Table 2 lists the summary of platform characteristics.

Table 2: Platform characteristics

W (N)	w (N)	L (m)	D(m)	σ_n(rad/s)	m (kg)
23×10^6	8000	500	50	1.3	2.9×10^6

The spring constant of the platform was determined as K = 5000 kN/m. The natural frequency of the platform is set at 1.3 rad/s. However, this value may vary based on changes in platform equipment weight and number of personnel working on deck. The damping ratio φ is supposedly determined experimentally with logarithmic decrement method. However, due to restricted environment in conducting on deck or otherwise experiment, the damping ratio has been determined by using the plots shown in Figure 3 by graphing the overdamped, critically damped, and underdamped conditions of the platform after following a smash by sea wave *A*.
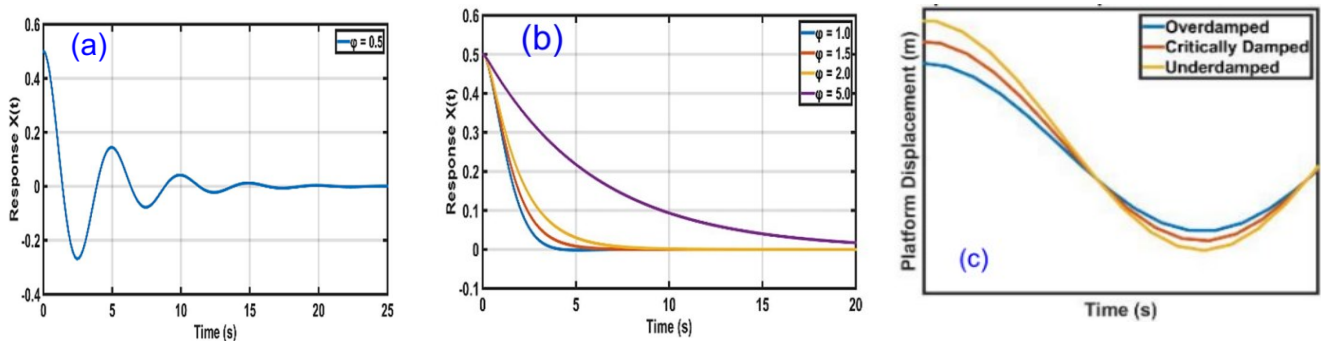

Figure 3: Graph of free response under-damped (a), and of critically damped and over damped, (b) of the TLP platform with initial displacement of 0.5 m. Figure 3(c) depicts the platform displacement under various damping.

The three figures shown above display the free response of TLP when acted upon by a one-time 120 kN force generated by the surge of sea wave *A* with an initial displacement of 0.5 m. The time taken for an under-damped TLP with $\varphi = 0.5$ to return to zero displacement is 20 s. However, the time taken for overdamped, and critically damped for a zero return is significantly quicker. In the case of critically damped when $\varphi = 1$, the time taken for TLP to return to zero displacement is 4.0 s while for the overdamped case or when $\varphi > 1$, the time taken for TLP to return to zero displacement

is more than 6.0 s. Thus, this work adopts the ideal case of critically damped vibration on the TLP for further analysis. The wave load by sea waves on the TLP is shown in Figure 4 (a) and (b). In Figure 4 (a), it is shown that the sea wave *A* loading on the TLP reaches 120 kN of force while the sea wave *B* loading shown in Figure 4 (b) reaches 2500 kN which is more than 20 times stronger than normal wave

loading. The pattern of wave loading shown in Figure 4 (a) shares similarity in shape and value with the results reported in Refs. [8, 10]. However, Ref. [8] results have significantly smaller wave loading value due to its scaled down prototype, which has smaller hull diameter and different platform natural frequency caused by different effective mass of the system.
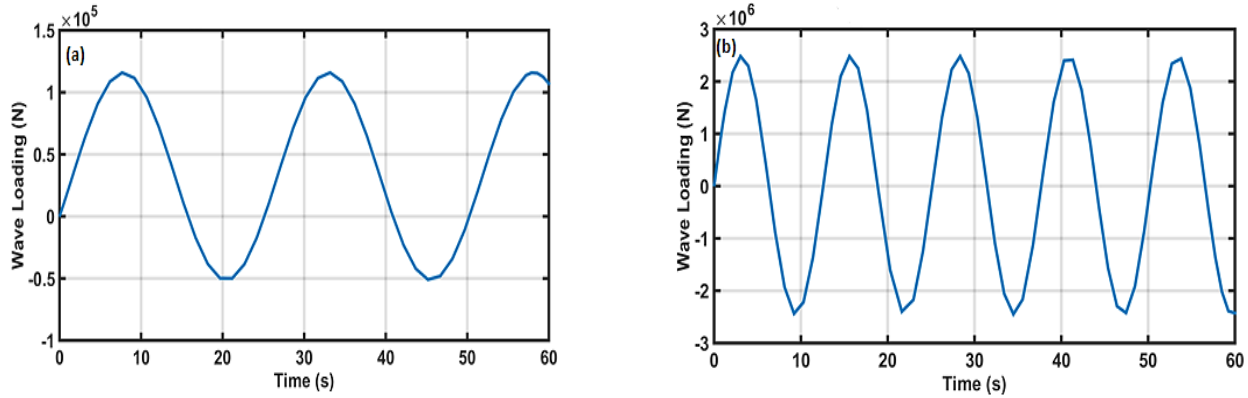

Figure 4: (a) sea wave *A* loading vs. time, and (b) sea wave *B* loading vs. time on the TLP.

The results from further analysis are shown in Figures 5 (b), for sea wave *A* and Figure 5 (b) for sea wave *B*, respectively. Note that for economy of space, we disregard Figures 5 (a) for both sea wave *A* and *B*. Sea wave *A* contributes a horizontal response to the platform under a normal wave travelling with a velocity amplitude of 25 m/s in 60 s. The peak displacement shown in the graph happens at time of 8 s, 34 s, and 58 s with a displacement approaching 0.02 m. The displacement shown in Figures 5 represents a similar pattern with that reported in [2] in terms of surge motion. However, the results shown here is more refined and less noisy in comparison to results of Ref. [2] where they use a CFD model that takes into consideration both wind and current load acting simultaneously on the TLP. Figure 5 also

exerts similarity related with results obtained in [11] with the highest amplitude reaching 0.08 m. However, there is a slight difference in the pattern of the platform movement due to different sea conditions. For sea wave *B*, the peak occurs more frequently at times of 4 s, 17 s, 28 s, 41 s, and 54 s, sequentially with a displacement of 0.5 m. The shorter peak-to-peak time span explains the sea wave *B* behavior, which has a higher frequency value and smaller wave period compared to sea wave *A*. The amplitude of the displacement increases linearly proportional to the wave loading. This shows that the wave loading on the TLP is directly proportional to its horizontal displacement. The maximum displacement value obtained from sea wave *B* is quite similar to the surge pattern shown in [8].
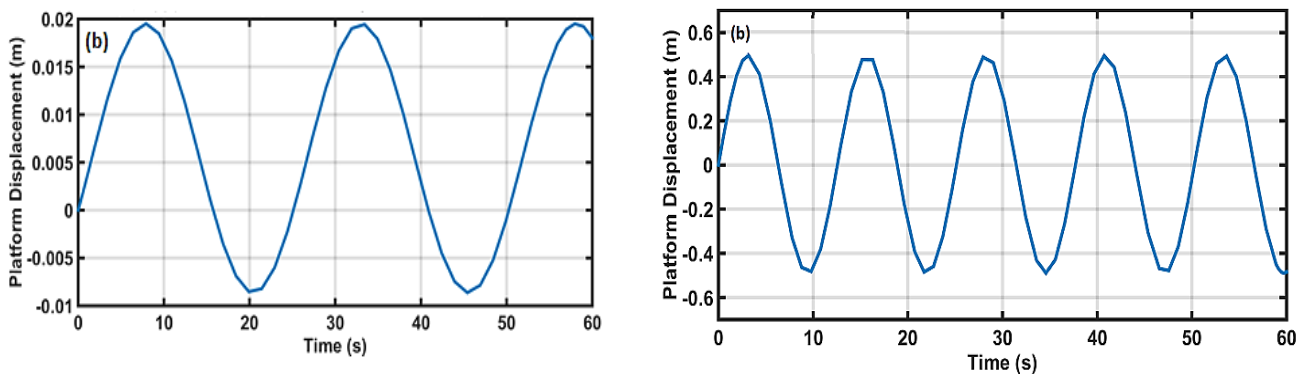

Figure 5: Platform displacement vs. time for TLP of sea waves *A* (right), and *B* (left) for 60 seconds.

In Figure 6, a direct assessment has been made to compare the significance of both sea waves *A* and *B* to the displacement of the TLP. The sea wave *B* loading is notably more dominant in contribution to the platform displacement with higher sea wave loading and greater frequency. On the other hand, a 0.02 m and 0.5 m of horizontal displacements

are insignificant compared to the actual size of the platform. However, one should be conscious of the fatigue limit of the tendons under such cyclic loading when designing the platform to withstand constant sea wave loadings on the platform for longer years of operation.
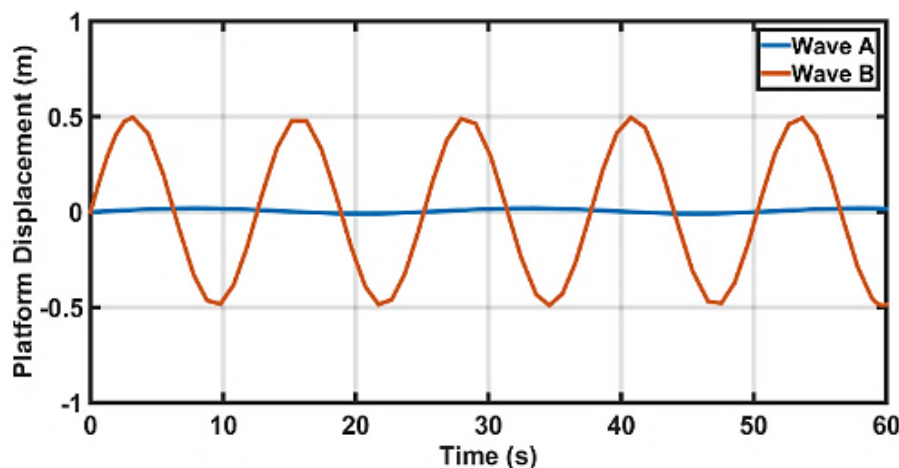
Figure 6: Direct comparison between sea wave *A* and sea wave *B* in term of period and amplitude.

Direct response of the platform under different sea wave velocity profiles are produced as shown in Figure 7. Figure 7 shows the platform displacement under the influence of different velocity profile ranging from 20 m/s to 30 m/s. It can be seen that as the velocity increases, the platform displacement slightly increases upward. The time taken for the platform to reach its maximum peak decreases as the velocity profile increases.
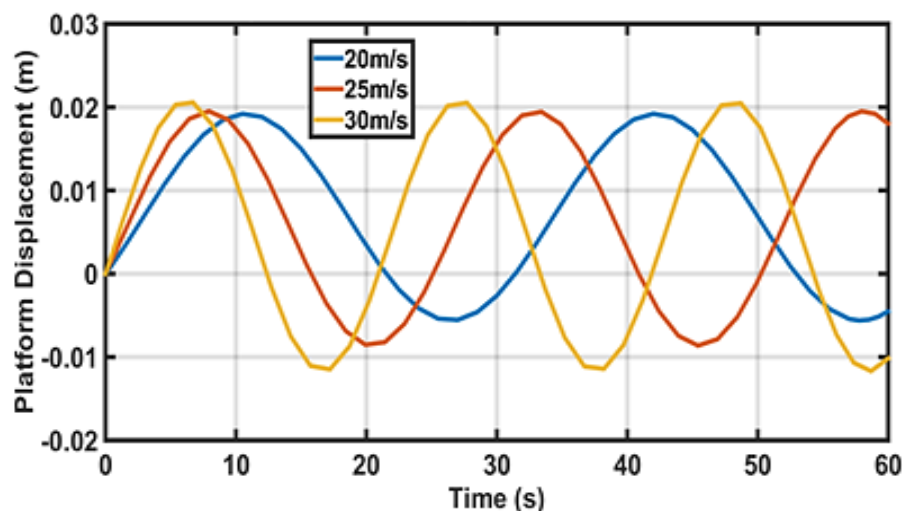

Figure 7: Platform displacement vs. time for the TLP at different velocity profile of sea wave *A*.

In Figure 7, we show that different velocity profile has an effect on the overall movement of the platform particular to the period of the cycle.

As the sea waves velocity increases, the time taken for the platform to return to initial position decreases. The time taken for the platform to complete one cycle for 20 m/s is 32 s, 25 m/s is 25 s whereas 30 m/s only takes 21 s.

Another point to take note of is the time taken for the displacement to reach its peak value decreases when velocity profile increases. This is due to higher velocity profile, which exert more force onto the platform tendons, allowing the platform to move at a faster rate compared to low velocity sea wave. The displacement amplitude increases as the velocity increases because higher velocity sea waves encompass higher energy level that generates a higher force when acted upon the TLP hull. It also creates larger displacement compared to low velocity sea waves.

This phenomenon supports the law of conversation of energy, and Newton's second law where higher velocity profile sea waves with higher kinetic energy eventually produces higher net force to transfer to the hull during impact thus, increases the displacement of the platform.

The displacement amplitude of the 30 m/s sea waves reaches approximately 0.021 m while the lower velocity profile 20 m/s sea waves only reaches its peak at 0.018 m.
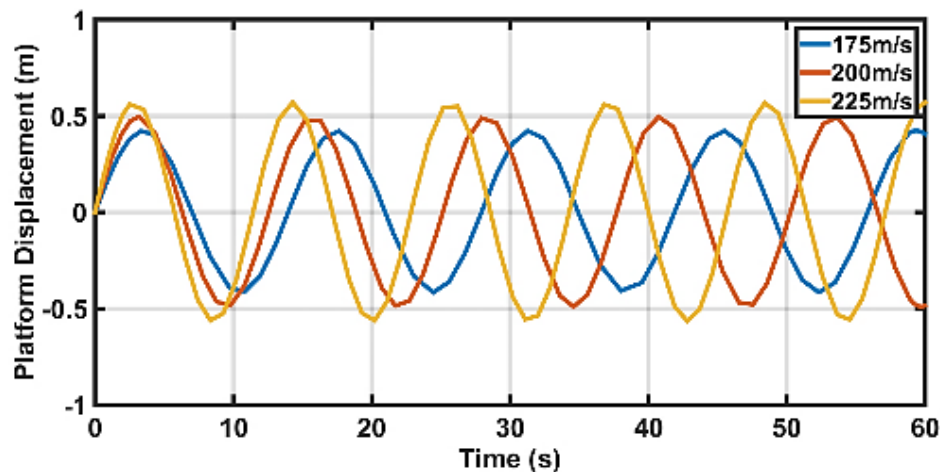
Figure 8: Platform displacement vs. time of the TLP for different velocity profile of sea wave **B**.

In Figure 8, we show similar pattern to Figure 7 with different displacement amplitudes. As the sea waves velocity increases, the time taken for the platform to return to initial position decreases. The time taken for the platform to complete one cycle for velocity of 175 m/s is 15 s, for 200 m/s is 13 s whereas the 225 m/s velocity only takes 11 s for a complete cycle.

The displacement amplitude increases as the velocity increases which is similar to Figure 7. This phenomenon again supports the law of conversation of energy, and Newton's second law. The displacement amplitude of the 225 m/s sea wave extents to approximately 0.6 m while the lower velocity profile of 175 m/s of this sea wave only scopes its peak at 0.4 m.

As shown in Figure 9, the resonance frequency of the TLP and the sea waves occurs at the natural frequency of 21 Hz, and 460 Hz regardless of the type of wave profile colliding with the TLP.

However, when sea wave **A** collides with the platform, the frequency profile of the TLP contains more noise compared to when sea wave **B** smashes onto the TLP. The frequency profile of the TLP under sea wave **B** shows more compactness and uniformity. By comparing the amplitude of both sea wave **A** and **B**, it is clear that sea wave **B** endeavors a higher amplitude when it reaches frequencies at approximately 21 Hz and 460 Hz, which are the resonance frequencies of the wave as well as the platform. Therefore, it is important to consider the value of resonance frequency during design stage of the TLP and tendons alike.

If taken to full capacity, platform resonance can cause catastrophic damages to the tendons due to vigorous horizontal movement. In comparison with previous investigations, our results exhibit similar pattern with several findings such as in [27-29].

However, these papers show slightly different results in terms of amplitude and resonance frequency. This is because different platforms may vibrate at their own unique frequencies.

Their overall response may also differ due to difference in size, mass, and structure. The difference in sea state and sea wave frequency may also contribute to dissimilarity in results of this work in contrast to findings published by other researchers. Different oceanic waves in different part of the world have their frequency and period based on weather conditions and geological effects.

It can be seen that different velocity profile does not affect the natural frequency of the platform. All three different velocity profiles when acted upon the platform reach resonance frequency at approximately 21 Hz and 460 Hz, respectively.

All sea waves reach resonance state at 21 Hz regardless of the velocity of the wave. However, the 30 m/s wave velocity profile shows a unique resonance frequency at 457 Hz. The deviation of data is still acceptable as it is still in the range of 460 Hz. However, this slight change in frequency value may indicate the possibility that the resonance frequency of the platform changes as the velocity of the wave increases beyond 30 m/s for a normal sea wave such as wave **A**.

Theoretically, a single degree-of-freedom spring mass damper system only contains one dominant natural frequency. The following scenario may explain the presence of two natural frequencies. Mathematically, the equation of motion of a continuous flexible structure such as the hull tendon has an infinite number of vibration modes, which gives the possibility of different natural frequencies with the platform hull.

Acceleration, velocity, and displacement of the TLP are governed by the transient state of the vibrating tendons. This reflects the act of forced vibration of a single-degree-of-freedom system. At the same time, the generalized Morison equation $F'(t)$ acts as the force function for the steady-state vibration of TLP. Hence, vibration of the whole structure experiences several modes, which in turn produces several natural frequencies.
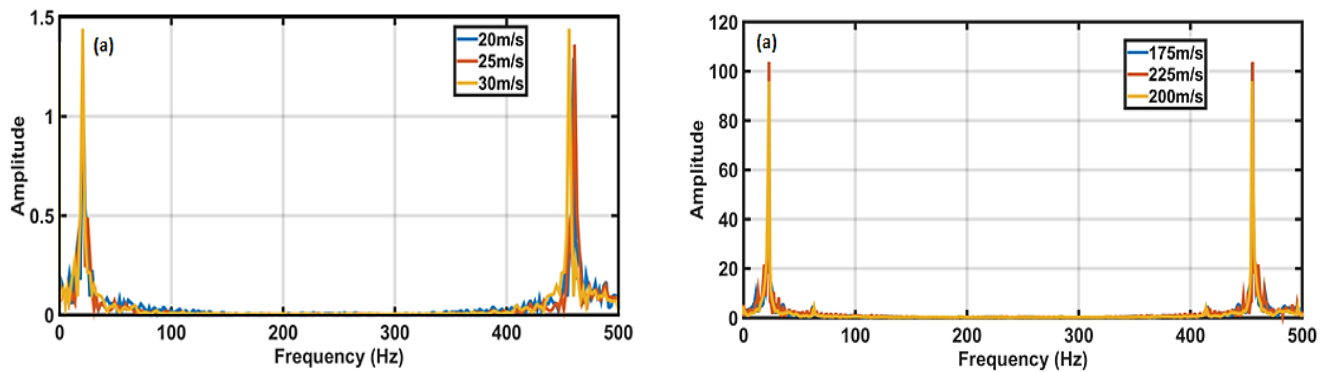
Figure 9: Frequency response of the TLP with different velocity profiles for sea waves *A* and *B*, respectively.

CONCLUSIONS

Analytical procedure to calculate the dynamic response of the TLP using a single-degree-of-freedom spring mass damper system has been established to determine the matter of sea wave impact on the horizontal movement of the platform that may eventually lead to slacking of tendons. Modified Morison wave equation has been integrated into the equation of motion of the platform to obtain the wave loading and the horizontal displacement of the TLP due to wave impact on the underside of the deck. In the event where a sea wave similar to wave *B* is encountered, the platform may experience substantial force, twenty times or greater than that of sea wave *A* with a possibility of 0.5 m horizontal displacement in the direction of wave propagation. This work also studied the consequence of different velocity profiles affecting the platform displacement. It can be concluded that as the velocity of the sea wave increases, the platform displacement amplitude increases, together with shorter period to reach the peak displacement value and

shorter time to return to original position. However, it does not convince that the smaller wave is safe in the analysis as smaller sea waves with lesser natural period may approach resonance frequency with the platform, which is approximately 21 Hz, and 460 Hz, as determined. It is possible that horizontal displacement of the TLP could exceed the results shown in this work upon resonance frequency. Different velocity profiles have no noticeable influence to bring about changes to the natural frequency of the platform.

A CFD simulation was produced using Star-CCM+ to show the possible dynamic response of the TLP when acted upon by sea wave *A*. these results point to the possibility to select a lighter material with greater resilience to strain from rogue sea waves so as to prolong the life cycle of the tendons. However, details on materials selection and vertical stress distribution of tendons is not covered as this work focuses on the vibrational aspects of the TLP which is to compute the possible dynamic response of the TLP under sea wave impacts.

REFERENCES

[1] H. A. Bourne Jr and M. Salama, "Mooring system for tension leg platform," ed: Google Patents, 1980.

[2] G. Wu, H. Jang, J. W. Kim, W. Ma, M.-C. Wu, and J. O'Sullivan, "Benchmark of CFD modeling of TLP free motion in extreme wave event," in *International Conference on Offshore Mechanics and Arctic Engineering*, 2014, vol. 45400, p. V002T08A086: American Society of Mechanical Engineers.

[3] D. I. Karsan and Z. Demirbilek, "Method and apparatus to stabilize an offshore platform," ed: Google Patents, 1990.

[4] I. W. S. Rawles, A. C. Kyriakides, S.-C. Li, Q. Ling, and G. Miao, "Tension Leg Platform With

Improved Hydrodynamic Performance," ed: Google Patents, 2011.

[5] A. A. Taflanidis, C. Vetter, and E. J. A. O. R. Loukogeorgaki, "Impact of modeling and excitation uncertainties on operational and structural reliability of tension leg platforms," vol. 43, pp. 131-147, 2013.

[6] A. J. O. E. Jain, "Nonlinear coupled response of offshore tension leg platforms to regular wave forces," vol. 24, no. 7, pp. 577-592, 1997.

[7] H. Lee, W.-S. J. J. o. S. Wang, and vibration, "Analytical solution on the dragged surge vibration of tension leg platforms (TLPS) with wave large body and small body multi-interactions," vol. 248, no. 3, pp. 533-556, 2001.

[8] R. Adrezin and H. J. P. E. M. Benaroya, "Response of a tension leg platform to stochastic wave forces," vol. 14, no. 1-2, pp. 3-17, 1999.

[9] C. A. Brebbia and S. Walker, *Dynamic analysis of offshore structures*. Newnes, 2013.

[10] S. M. G. Zadeh, R. S. Baghdar, and S. M. S. V. K. J. O. J. o. M. S. Olia, "Finite element numerical method for nonlinear interaction response analysis of offshore jacket affected by environment marine forces," vol. 5, no. 04, p. 422, 2015.

[11] A. A. M. Ali, A. Al-Kadhimi, and M. J. J. J. o. C. E. Shaker, "Dynamic behavior of jacket type offshore structure," vol. 6, no. 4, pp. 418-435, 2012.

[12] D. Kelly and A. Coddington, *The Bermuda Triangle, Stonehenge, and Unexplained Places*. Cavendish Square Publishing, LLC, 2017.

[13] D. C. J. P. A. R. Menzel, "The Katrina aftermath: A failure of federalism or leadership?," vol. 66, no. 6, pp. 808-812, 2006.

[14] M. Rudman and P. W. J. O. E. Cleary, "Rogue wave impact on a tension leg platform: The effect of wave incidence angle and mooring line tension," vol. 61, pp. 123-138, 2013.

[15] T. Johannessen, S. Haver, T. Bunnik, and B. J. P. D. O. T. Buchner, "Extreme wave effects on deep water Tlps lessons learned from the Snorre a model tests," pp. 28-30, 2006.

[16] J. Morison, J. Johnson, and S. J. J. o. P. T. Schaaf, "The force exerted by surface waves on piles," vol. 2, no. 05, pp. 149-154, 1950.

[17] W. C. Nolan and V. C. Honsinger, "Wave-induced vibrations in fixed offshore structures," Massachusetts Institute of Technology, 1962.

[18] S. Chandrasekaran, A. Jain, and N. J. O. E. Chandak, "Influence of hydrodynamic coefficients in the response behavior of triangular TLPs in regular waves," vol. 31, no. 17-18, pp. 2319-2342, 2004.

[19] R. Burrows, R. Tickell, D. Hames, and G. J. A. O. R. Najafian, "Morison wave force coefficients for application to random seas," vol. 19, no. 3-4, pp. 183-199, 1997.

[20] N. J. E. J. o. S. E. Haritos, "Introduction to the analysis and design of offshore structures–an overview," no. 1, pp. 55-65, 2007.

[21] N. Veritas, *Environmental conditions and environmental loads*. Det Norske Veritas Oslo, Norway, 2000.

[22] S. S. Rao, "Mechanical Vibrations, Pearson Education Inc," in *6th ed. s.l* 2018.

[23] N. Abdussamie, R. Ojeda, Y. Drobyshevski, G. Thomas, W. J. S. Amin, and O. Structures, "Experimental investigation of extreme wave impacts on a rigid TLP model in cyclonic conditions," vol. 12, no. 2, pp. 153-170, 2017.

[24] ed, pp. http://www.shell.com/about-us/major-projects/malikai.html.

[25] J. N. Sharma, S. Tryggestad, and J. Bian, "A comprehensive wind, wave and current measurement program in the South China Sea," in *Coastal Engineering 1996*, 1997, pp. 354-367.

[26] N. H. Idris, M. Seeni, and I. Mohd, "Sea surface current circulation pattern in the South China Sea derived from satellite altimetry," in *Proceedings of the 28th Asian Conference on Remote Sensing*, 2007.

[27] V. Jaksic *et al.*, "Dynamic response mitigation of floating wind turbine platforms using tuned liquid column dampers," vol. 373, no. 2035, p. 20140079, 2015.

[28] X. Chen, Y. Ding, J. Zhang, P. Liagre, J. Niedzwecki, and P. J. O. E. Teigen, "Coupled dynamic analysis of a mini TLP: Comparison with measurements," vol. 33, no. 1, pp. 93-117, 2006.

[29] O. Nwogu and M. Irani, "Numerical prediction of higher order wave induced loads on tethered platforms," in *The First ISOPE European Offshore Mechanics Symposium*, 1990: OnePetro.